Functionalized *N*-Heterocyclic Carbene Monolayers on Gold for Surface-Initiated Polymerizations

Yunsoo Choi, Chul Soon Park, Hung-Vu Tran, Chien-Hung Li, Cathleen M. Crudden, and T. Randall Lee*

Cite This: *ACS Appl. Mater. Interfaces* 2022, 14, 44969−44980

Read Online

ACCESS | Metrics & More | Article Recommendations | Supporting Information

ABSTRACT: Although *N*-heterocyclic carbenes (NHCs) are superior to thiol adsorbates in that they form remarkably stable bonds with gold, the generation of NHC-based self-assembled monolayers (SAMs) typically requires a strong base and an inert atmosphere, which limits the utility of such films in many applications. Herein, we report the development and use of bench-stable NHC adsorbates, benzimidazolium methanesulfonates, for the direct formation of NHC films on gold surfaces under an ambient atmosphere at room temperature without the need for extraordinary precautions. The generated NHC SAMs were fully characterized using ellipsometry, X-ray photoelectron spectroscopy (XPS), polarization modulation infrared reflection-absorption spectroscopy (PM-IRRAS), and contact angle measurements, and they were compared to analogous SAMs generated from an NHC bicarbonate adsorbate. Based on these findings, a unique radical initiator α,ω-bidentate azo-terminated NHC adsorbate, **NHC15AZO[OMs]**, was designed and synthesized for the preparation of SAMs on gold surfaces with both NHC headgroups bound to the surface. The adsorbate molecules in **NHC15AZO** SAMs can exist in a hairpin or a linear conformation depending on the concentration of the adsorbate solution used to prepare the SAM. These conformations were studied by a combination of ellipsometry, XPS, PM-IRRAS, and scanning electron microscopy using gold nanoparticles (AuNPs) as a tag material. Moreover, the potential utility of these unique radical-initiating NHC films as surface-initiated polymerization platforms was demonstrated by controlling the thickness of polystyrene brush films grown from azo-terminated NHC monolayer surfaces simply by adjusting the reaction time of the photoinitiated radical polymer growth process.
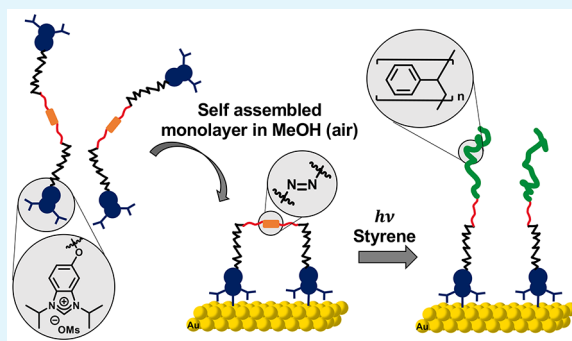
INTRODUCTION

Surface modification by grafted polymer brushes has emerged as a powerful technology for tuning the physical and chemical properties of interfaces, and it has facilitated progress in multiple interface applications, including antifouling coatings,[1−3] nanoscale sensors,[4,5] energy storage,[6] catalysis,[7] and nanochannels.[8] In general, thin polymer films, so-called polymer brushes, are polymer chains with end groups tethered onto a solid interface.[9] Such thin films can be generated by adsorbing presynthesized polymers onto a surface (grafting to) or by growing polymers from surfaces (grafting from). Although the grafting to method is generally used to fabricate polymer brushes due to its experimental simplicity, grafting from techniques are more favorable because they can lead to higher grafting densities and greater film thicknesses.[10]

Surface-initiated polymerizations (grafting from) typically require initiator groups anchored on the surface to grow polymers directly from substrates. Although several types of initiator-terminated adsorbates have been developed for use on various substrates, most studies have focused on Au[1,11,12] or silica.[7,13] Developing a method for surface-grafted polymerizations from self-assembled monolayers (SAMs) derived from the adsorption of organothiols on gold offers several advantages compared to SAMs derived from the adsorption of organosilanes on silica. First, organothiol SAMs on gold are easy to form, well defined, and well studied.[14] Second, SAMs on gold offer surfaces composed of readily selectable chemical functionalities depending on the terminal species of the adsorbate used, which can be used to tune the interfacial
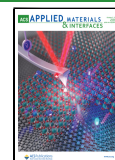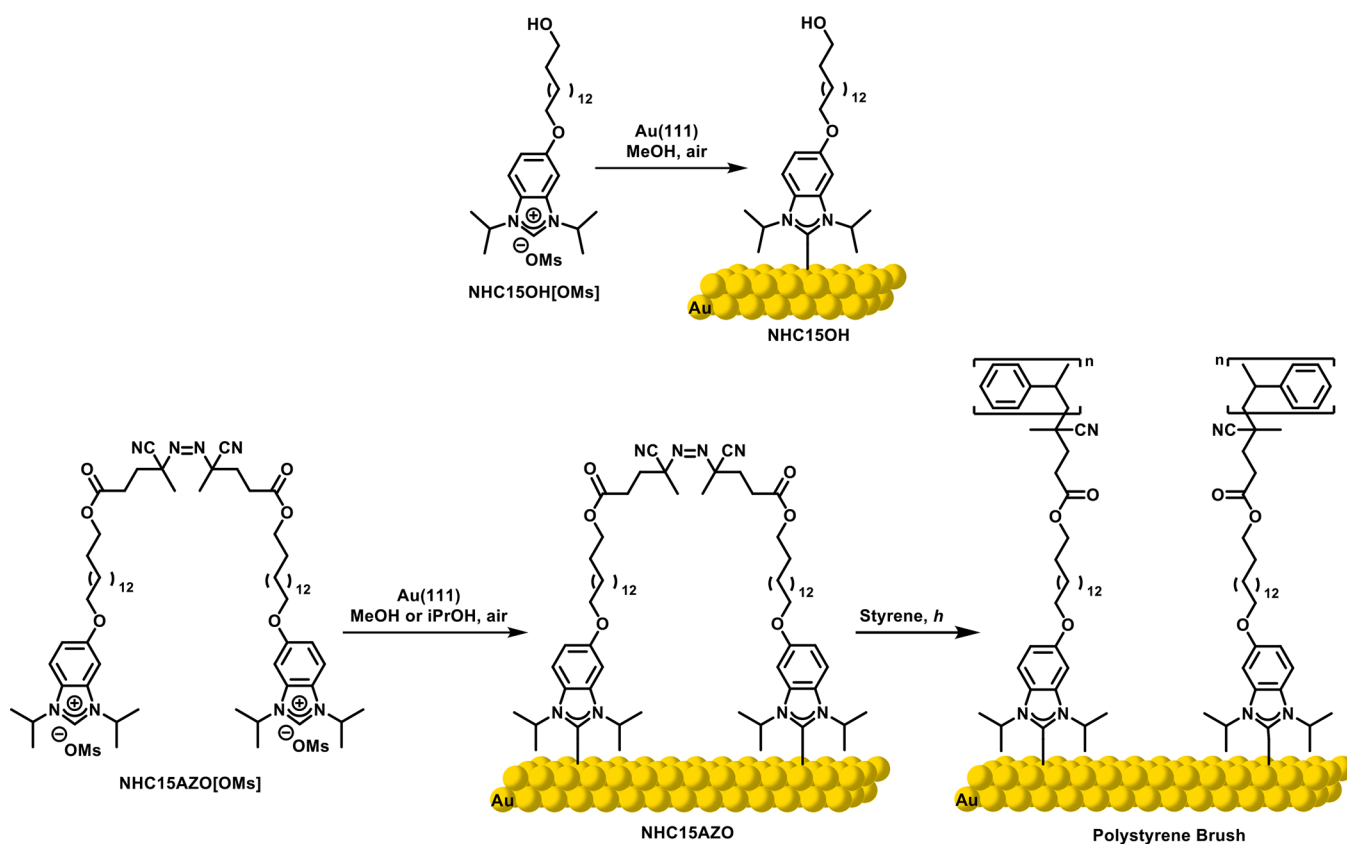
Scheme 1. Molecular Structure of the NHC15OH[OMs] Adsorbate and the Corresponding SAM Formation on the Surface of Gold (Top). Molecular Structure of the NHC15AZO[OMs] Adsorbate, the Corresponding SAM, and Polystyrene Brush on the Surface of Gold (Bottom)
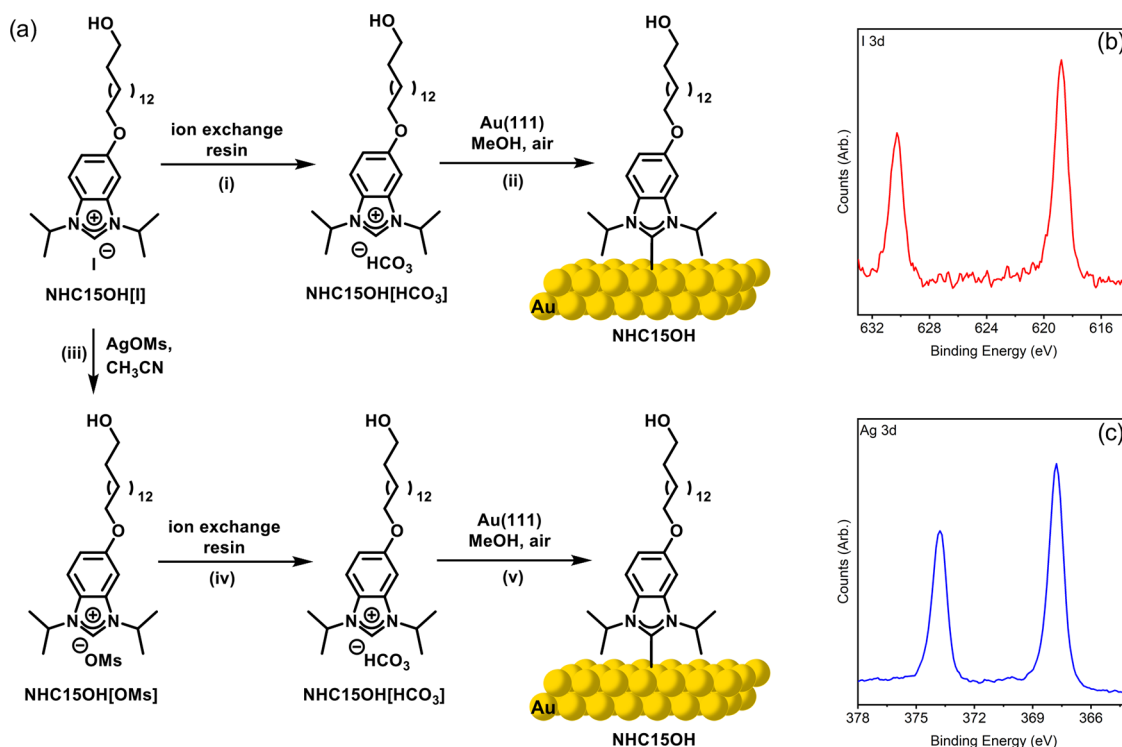

properties in a controllable fashion.[15−17] Moreover, organic SAMs on gold have the capacity to utilize surface plasmon resonance (SPR) effects for useful applications (e.g., in biosensing).[18] Thus, surface modifications, including polymerizations via SAM formation, have been investigated mainly using thiol absorbates, despite the instability of Au−S bonds at temperatures higher than ∼80 °C and under oxidizing conditions.[19−21]

As a more stable anchoring headgroup, *N*-heterocyclic carbenes (NHCs) have recently generated substantial interest in the functionalization of Au surfaces.[22−24] NHCs form a bond with gold that is remarkably more stable (∼40 kcal/mol) than Au−S bonds (∼30 kcal/mol), and they are synthetically versatile due to their compatibility with various organic functional groups.[20] In fact, the Crudden group found that SAMs generated from NHCs are more chemically, thermally, and electrochemically stable than thiol-derived SAMs on gold.[19] Despite these attractive features, the major drawback to forming SAMs on gold via carbene adsorption is the contamination of residual amines from the strong bases (e.g., KHMDS) used to produce free carbenes; such residues limit the formation of well-ordered SAMs because these residual amines can bind strongly to the metal surface.[25,26] The most successful efforts to overcome this disadvantage have been concentrated on using "masked NHCs", which can generate free carbenes without the use of strong bases.[27] Specifically, the Crudden group reported the preparation and deposition of benzimidazolium hydrogen carbonate salts, which are "masked NHCs", on gold surfaces.[20,28,29] In these studies, bench-stable NHC bicarbonate-based adsorbates were prepared via ion-

exchange. Gold slides were then immersed into solutions of the NHC bicarbonate-based adsorbates under an ambient atmosphere, which led to self-assembly of the adsorbates into thin films on the gold surfaces. However, the studies related to NHC-based SAMs on flat gold surfaces thus far have mostly focused on the configurations of NHC adsorbates on gold surfaces using experimental and computational methods.[30−35] Until now, there have been only limited examples of functionalized NHC SAMs and their applications,[22] including biosensors,[36,37] microprinting,[38] organic electronics,[39−41] photoswitches,[42] and polymerization.[25,26]

In this study, we report a new method for the direct formation of functionalized NHC-based monolayers on gold and utilized azo-initiated NHC SAMs for growing polymer brushes from gold surfaces based on this newly developed method. This method includes three steps: (i) development of the bench-stable benzimidazole methanesulfonate-based adsorbates and optimization of their SAM formation on gold, (ii) generation and characterization of azo-initiator NHC SAMs on gold, and (iii) surface-initiated polymerizations from the azo-radical initiated NHC monolayers. Specifically, we synthesized 1,3-diisopropyl-6-((15-hydroxypentadecyl)oxy)-1*H*-benzo[*d*]-imidazol-3-ium methanesulfonate (**NHC15OH[OMs]**) and optimized the conditions for the direct formation of its monolayers on gold, as illustrated in Scheme 1 (top). The formation of NHC SAMs from our NHC[OMs] adsorbates not only prevents possible contamination of the gold surface by the residuals of bases or incomplete ion exchange but also prevents the degradation of the functional groups of the NHC-

Scheme 2. Challenges in the Deposition of NHC Adsorbates to Generate Organic Thin Films[a]

[a](a) Illustration of the procedures used to deposit NHC adsorbates on the gold employed ion-exchange step. (b) I 3d region of the XPS spectrum of the film generated through steps (i) and (ii). (c) Ag 3d region of the XPS spectrum of the film generated through steps (iii−v).

based adsorbates and facilitates the synthesis of NHCs containing complex functional groups.

The optimized conditions were then applied to generate azo-functionalized NHC thin films for polymer brush growth on gold surfaces. We synthesized the azo-initiator adsorbate 6-((15-((4-cyano-4-((2-cyano-5-((14-((1,3-diisopropyl-1H-benzo[d]im-idazol-3-ium-5-yl)oxy)tetradecyl)oxy)-5-oxopentan-2-yl)diazenyl)pentanoyl)oxy)pentadecyl)oxy)-1,3-diisopropyl-1H-benzo[d]imidazol-3-ium methanesulfonate (**NHC15AZO[OMs]**), as shown in Scheme 1 (bottom). The designed adsorbate has two unique features: (i) NHC headgroups to improve the thermal and oxidative stability of the SAMs on gold and (ii) an α,ω-bidentate architecture to tether all of the azo radical initiator sites to the surface; consequently, no surface-unbound free polymer chains would be generated during polymer growth. Such free polymer species sometimes adhere to the growing polymer films and cannot be removed easily, and they affect the quality of the surface-grafted polymer brushes.[11] Moreover, we examined **NHC15AZO** SAMs generated from solutions with systematically varying concentrations (0.01, 0.10, and 1.00 mM) of the **NHC15AZO[OMs]** adsorbate to investigate the effect of the adsorbate concentration on the conformations of the related NHC monolayers on gold (hairpin vs linear). The monolayers were characterized by optical ellipsometry, X-ray photoelectron spectroscopy (XPS), polarization modulation infrared reflection-absorption spectroscopy (PM-IRRAS), contact angle goniometry, and scanning electron microscopy (SEM). Importantly, the potential application of our newly developed system was illustrated by growing polystyrene brushes via photoinitiated polymerization under irradiation using UV 365 nm light.

EXPERIMENTAL SECTION

Complete details regarding the materials, procedures, and instrumentation used to perform the research reported in this manuscript are provided in the Supporting Information.

RESULTS AND DISCUSSION

Development of the NHC15OH[OMs] Adsorbate and Its Formation of Thin Films on Gold. To deposit NHCs on gold surfaces to generate monolayers, free NHCs are typically prepared *in situ* using base deprotonation of imidazolium halogen salts in an air-free and water-free environment.[19,25,32,34,40−43] However, base residues prevent the formation of well-ordered NHC SAMs;[44] additionally, the **NHC15AZO**-based molecule, the target adsorbate to be deposited on gold surfaces for surface-anchored polymerizations, possesses ester functional groups that are labile under such conditions due to transesterification reactions that occur in the presence of strong bases.[45] An alternative method has been explored to deposit NHC SAMs on gold surfaces using NHC bicarbonate or NHC-CO$_2$ adduct precursors via vapor deposition under vacuum conditions.[20,30,31,35,38,46] The use of such bicarbonate or CO$_2$ adduct forms, called "masked NHCs", has been an attractive strategy because they are relatively stable under air, and CO$_2$ and H$_2$O are the only byproducts upon the generation of free NHCs to form SAMs on Au surfaces.[27,47] Although this approach enables the formation of well-ordered monolayers without contamination issues, the addition of heat during the preparation of the NHC-CO$_2$ adduct precursors is unsuitable for our targeted azo-functionalized **NHC15AZO** precursor because the azo groups decompose at high temperatures.[48] Alternatively, the bicarbonate form of "masked NHC" adsorbates can be prepared

under mild conditions from the iodide salts of their imidazolium/benzimidazolium precursors after treatment with an ion-exchange resin.[20,36,37,39] Thus, we synthesized **NHC15OH** iodide (**NHC15OH[I]**) and converted it to **NHC15OH[HCO$_3$]** to identify the deposition conditions for NHC SAM formation (Scheme 2a, steps (i) and (ii)).

The challenge with the ion-exchange procedure is that it can be difficult to assess the completeness of the procedure without relying on elemental analysis, and the transformation can be further challenging with more structurally complex NHCs such as **NHC15OH**, which is shown in Scheme 2a. To examine the effectiveness of the iodide exchange, we prepared SAMs from ion-exchanged **NHC15OH[HCO$_3$]** as in Scheme 2a, step (ii) and probed their elemental composition by X-ray photoelectron spectroscopy (XPS). This technique enables the determination of the chemical compositions of the SAMs based on the binding energies of the various elements present in the SAM.[49,50] The I 3d region of the XPS spectrum, which ranges from 612 to 634 eV, was specifically examined, and it was found that the SAMs contained a substantial amount of iodide, as shown in Scheme 2b. It is known that iodide strongly adsorbs on the Au(111) facets,[51,52] leading to uncontrolled SAM quality. For further confirmation of the monolayer quality, ellipsometric thicknesses of alkyl-terminated **NHC15** SAMs on gold generated by a similar procedure (Figure S1) were measured. As shown in Figure S1, 35 different samples of **NHC15** SAMs were prepared, and their corresponding thicknesses varied in the range of 1−11 Å. Thus, we were unable to obtain high-quality NHC SAMs from the bicarbonate form of both "masked NHC" adsorbates **NHC15OH[HCO$_3$]** and **NHC15[HCO$_3$]** prepared from the iodide salts of their NHC precursors and treatment with ion-exchange resin.

To attempt complete removal of iodide in NHC SAMs, we performed a salt metathesis reaction of **NHC15OH[I]** with silver methanesulfonate (**AgOMs**) to form **NHC15OH[OMs]** after removing the precipitated silver iodide (Scheme 2a, step (iii)). A subsequent ion-exchange step in a methanolic solution generated the desired **NHC15OH[HCO$_3$]** adsorbate, which was then used for monolayer formation (Scheme 2a, steps (iv) and (v)). Although these samples were devoid of iodide, the films generated by this route were contaminated with silver, detected in the Ag 3d region of XPS spectra from 378 to 363 eV, as shown in Scheme 2c.

Considering the contamination challenges mentioned above, we then attempted to form SAMs on gold from an NHC precursor prepared without iodide but with an apparently innocent counterion. As shown in Scheme 3, **NHC15OH-**

[OMs] adsorbates were directly synthesized from commercially available 2-propyl methanesulfonate and compound **1** (the detailed synthetic procedures are described in Scheme S1 in the Supporting Information). Interestingly, direct deposition of the bench-stable **NHC15OH[OMs]** adsorbate allowed for the formation of high-quality **NHC15OH** thin films on gold surfaces when Au slides were immersed in methanol solutions of **NHC15OH[OMs]** under an atmosphere of air at room temperature for 24 h, as shown in Scheme 3 and described in the following sections.

To compare the quality of SAMs generated from the **NHC15OH[OMs]** and **NHC15OH[HCO$_3$]** adsorbates, **NHC15OH[HCO$_3$]** was synthesized through ion exchange of the **NHC15OH[OMs]** compound using an ion-exchange resin, and the corresponding **NHC15OH** SAMs were prepared in methanol solutions. **NHC15OH** SAMs generated from the **NHC15OH[OMs]** and **NHC15OH[HCO$_3$]** adsorbates were characterized by four different surface characterization techniques, with each characterization experiment conducted at least three times. The data are summarized in Table 1.

First, preliminary confirmation of the presence of SAMs on the gold substrates was evaluated by measuring the SAM thickness using ellipsometry (see Figure S2a,b). The thickness of the monolayers derived from **NHC15OH[OMs]** was 11 Å, which is the same as that of the films generated from **NHC15OH[HCO$_3$]** within the experimental error. Next, the N 1s spectra of the monolayer generated from **NHC15OH[OMs]** and **NHC15OH[HCO$_3$]** were curve-fitted, as shown in Figure S2c. The peaks found at 399.8 eV indicate that both the **NHC15OH[OMs]** and **NHC15OH[HCO$_3$]** adsorbates were covalently bound to the gold surface, and this finding is consistent with other reported benzimidazole-based SAMs on gold (400.2−400.6 eV),[35,38,42,43] although the peaks are shifted by 0.4−0.8 eV. Such a shift to higher binding energy in these SAMs can plausibly arise from charge depletion at the N atoms in the NHC monolayers due to the interaction of their π-electron system with the Au substrate.[31,35]

In the **NHC15OH** SAMs, the alkyl chains on the benzimidazole moieties help to maximize interchain van der Waals interactions, allowing the molecules within these SAMs to have an upright orientation, and insufficient chain−chain interactions lead to more flat-lying adsorbate structures on the substrate.[53] Polarization modulation infrared reflection-absorption spectroscopy (PM-IRRAS) is a useful technique that can be used to evaluate the conformational order or crystallinity of alkyl chains in SAMs.[15,49,54] Specifically, the positions of the asymmetric methylene C−H stretching vibration ($\nu_a^{CH_2}$) bands provide insight into the intermolecular environment of the alkyl chains in organic thin films.[55] For example, the peak position for the $\nu_a^{CH_2}$ in an octadecanethiol monolayer on gold, which is conformationally ordered with trans-extended chains, is ~2918 cm^{-1}, whereas this peak shifts to higher wavenumbers in films with more liquid-like structures due to the increase in gauche defects.[56,57] The peak positions for the asymmetric methylene C−H stretching in **NHC15OH** SAMs generated from both salts (**OMs** and **HCO$_3$**) were observed at 2927 cm^{-1}, as shown in Figure S2d, indicating that the NHC-based monolayers are less conformationally ordered than the thiol-based monolayers. Finally, the contact angles of water as the probe liquid were used to evaluate the interfacial properties of the two surfaces. The contact angles were ~80° for both monolayers (Figure S2e). Based on the data from ellipsometric, XPS, PM-IRRAS, and water contact angle measure-

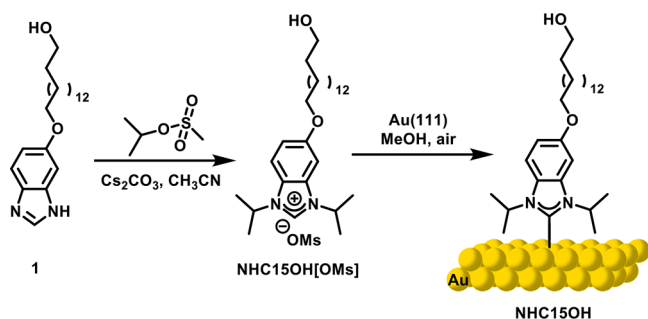**Scheme 3. Synthesis of the NHC15OH[OMs] Adsorbate and SAM Formation**

Table 1. Ellipsometric Thicknesses, N 1s XPS Peak Positions, PM-IRRAS Peak Positions of Asymmetric Methylene C–H Stretching, and Water Contact Angles of NHC15OH SAMs Generated from NHC15OH[OMs] and NHC15OH[HCO$_3$] Adsorbates

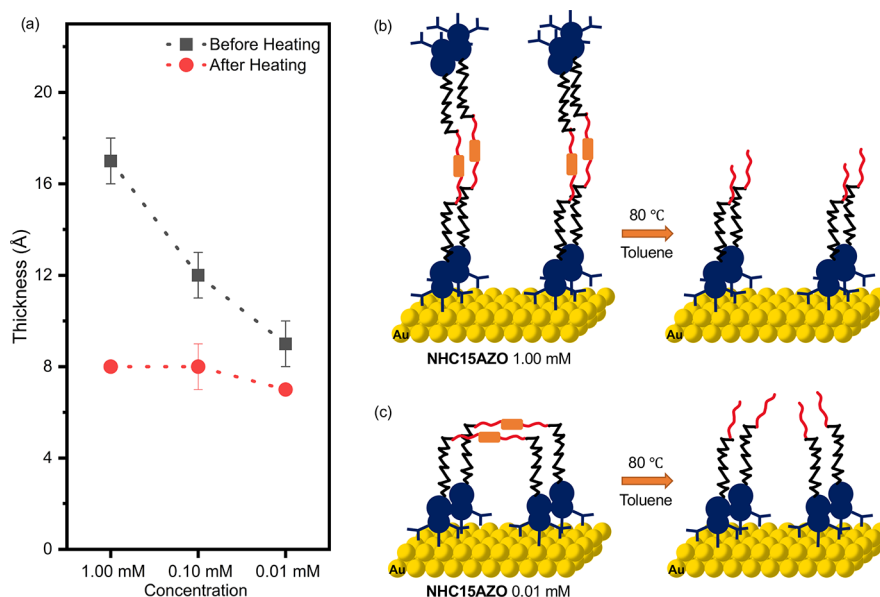| adsorbates	ellipsometric thickness	peak positions of N 1s from XPS	peak positions of $\nu_a^{CH_2}$ from PM-IRRAS	water contact angles
NHC15OH[OMs]	11 ± 2 Å	399.8 ± 0.3 eV	2927 cm^{-1}	80 ± 2°
NHC15OH[HCO$_3$]	12 ± 1 Å	399.8 ± 0.1 eV	2927 cm^{-1}	81 ± 2°

Figure 1. (a) Ellipsometric thicknesses of **NHC15AZO** monolayers generated from selected concentrations of adsorbate solutions before and after thermal treatment at 80 °C. Measurement of each thickness was based on three independent sets of experiments. Illustration of expected monolayer orientations generated from (b) 1.00 mM and (c) 0.01 mM **NHC15AZO[OMs]** in methanol and their corresponding structures after thermal treatment.

ments of these SAMs, we can conclude that the monolayers generated from the **NHC15OH[OMs]** were identical to the films derived from the bicarbonate-based carbene adsorbate **NHC15OH[HCO$_3$]**. Moreover, the elemental composition of both of these SAMs on gold was evaluated by examining their XPS survey spectra, which showed no detectable amounts of sulfur (Figure S3). Thus, the use of a benzimidazolium methanesulfonate adsorbates allows the direct formation of high-quality NHC thin films on gold without special precautions under an ambient atmosphere of air.

Generation and Characterization of the NHC15AZO Monolayer. In addition to the contamination of the SAMs with the use of NHC iodide salts, as shown in Scheme 2, the ester groups in **NHC15AZO[I]** underwent partial transesterification and generated hydroxy-terminated **NHC15OH-[HCO$_3$]** during the ion-exchange step (Scheme S2). The transesterification of esters with alkali metal carbonates is a common procedure.[58] In fact, after the ion exchange of the **NHC15AZO[I]** compound, a triplet peak was observed at 3.5 ppm in the ^{1}H NMR spectrum, which was assigned to the methylene group next to the hydroxyl group in the **NHC15OH[HCO$_3$]** compound (see Figure S4). Fortunately, the desired azo-initiator adsorbate **NHC15AZO[OMs]** was successfully synthesized from **NHC15OH[OMs]** via ester coupling with 4,4′-azobis(4-cyanopentanoic acid) in the presence of dicyclohexyl carbodiimide (a detailed synthesis procedure is illustrated in Scheme S1 in the Supporting Information). Notably, **NHC15AZO**-based SAMs were successfully prepared without transesterification from methanolic solutions of **NHC15AZO[OMs]** at room temperature

in the dark (Figure S5) and characterized by various surface characterization techniques.

Thickness Analysis. Figure 1a provides thickness data for the **NHC15AZO[OMs]** SAMs. Interestingly, the thickness of the SAMs generated from **NHC15AZO[OMs]** linearly increased with an increase in the concentration of the adsorbate solutions. The thickness of the **NHC15AZO** SAM generated from a 1.00 mM solution of the **NHC15AZO[OMs]** was 17 Å, which is almost double the thickness of SAMs obtained from the 0.01 mM solution (9 Å). Such behavior can plausibly arise from two different conformations of the **NHC15AZO** molecule on the surface of gold (hairpin vs linear).[11] In highly concentrated solutions (1.00 mM), one of the NHC headgroups binds to the gold substrate, while the other headgroup is exposed at the SAM surface, orienting as a linear construction of the **NHC15AZO** molecules. In contrast, at low concentrations (0.01 mM), both NHC headgroups bind to the gold substrate to form a hairpin structure. The expected orientations of monolayers obtained from solutions having varying concentrations of **NHC15AZO[OMs]** adsorbate are illustrated in Figure 1b,c.

To support the proposed orientation of molecules, as outlined in Figure 1b,c, additional thickness analyses were performed for the azo-initiator **NHC15AZO** monolayers generated from solutions of varying concentration. Specifically, each SAM was immersed in a glass vial containing 20 mL of toluene and then placed in an oil bath at 80 °C for 24 h. The films were removed from solution, cleaned, and dried before measuring their thickness. Not surprisingly, the thickness of all films was reduced to the same value of ~8 Å. According to
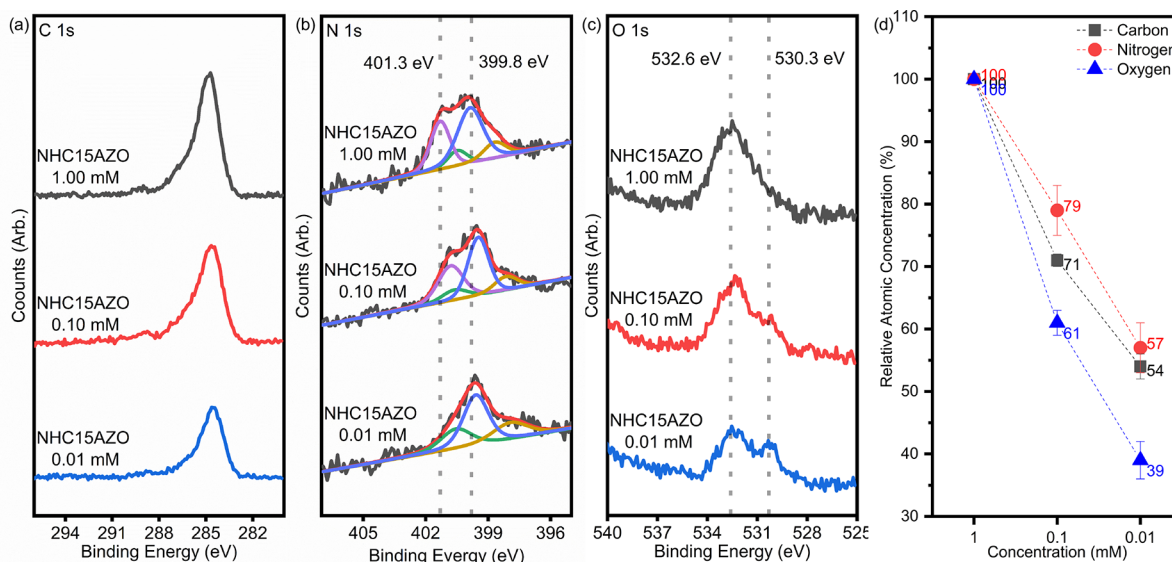
Figure 2. XPS spectra of **NHC15AZO** monolayers generated from 1.00, 0.10, and 0.01 mM MeOH solutions: (a) C 1s, (b) N 1s, and (c) O 1s. (d) Relative atomic concentration profiles of carbon, nitrogen, and oxygen as functions of the adsorbate solution concentration. Calculations of the percent of relative atomic concentrations were based on three independent sets of experiments.

previously reported thermal stability studies of NHC monolayers on gold substrates,[19,22] carbene-based films are stable at this temperature. Thus, no significant desorption of **NHC15AZO** from the surface would be expected during these thermal treatments. However, AIBN-type initiators easily decompose and generate nitrogen gas to produce two equivalent reactive radicals under these conditions.[48] As shown in Figure 1b, the SAM obtained from the 1.00 mM **NHC15AZO[OMs]** solution, which has a linear orientation on the surface, lost half of its atoms via fragmentation under thermal treatment, leading to a decrease in the thickness from 17 to 8 Å. In contrast, the film generated from the 0.01 mM solution retained almost of its atoms despite fragmentation on the surface due to their hairpin structure on gold substrates. Consequently, thermal treatment at 80 °C had little or no effect on the thickness of the film derived from the 0.01 mM solution, as shown in Figure 1c. Further phenomena related to the orientations of **NHC15AZO** on gold substrates will be discussed in subsequent sections.

XPS Analysis. The XPS spectra of the **NHC15AZO** films generated from selected adsorbate concentrations (1.00, 0.10, and 0.01 mM) are shown in Figure 2. The spectra reveal the presence of the C, N, and O elements in all monolayers. Figure 2a shows the C 1s spectra of the **NHC15AZO** monolayers generated from each adsorbate concentration. The C 1s spectra of the 1.00 mM **NHC15AZO** film were fitted with four different components: the peaks at 284.8, 286.3, 287.4, and 289.1 eV are attributed to the C−C, C−O/C−N, C≡N, and C═O species, respectively (Figure S6).[38,39,59,60] Quantitative analysis of the C 1s peaks will be discussed in detail below.

In addition to the elemental analysis of the surfaces, the degree of surface binding of atoms/functional groups was determined using spectral peak fitting. For example, the binding energies of the S 2p peaks in thiol-based SAMs on gold allowed for the determination of the degrees of bound and unbound sulfur species by comparing the ratio of peaks at ∼162 and ∼164 eV for bound and unbound thiols, respectively.[49] In a similar study, the XPS spectra of the N 1s core level of the **NHC15AZO** films generated at various

adsorbate concentrations were obtained (Figure 2b). The N 1s spectrum of the 1.00 mM **NHC15AZO** monolayer was fitted with four different peaks, as shown in Figure S7. The peaks at 398.8 and 400.6 eV correspond to nitrile (C≡N) and azo (N═N) nitrogens, respectively.[59,61] The peak observed at 399.8 eV corresponds to the NHC groups that are covalently bound to the gold substrate, which is in good agreement with the **NHC15OH** SAMs (Figure S2). The peak position at 401.3 eV can be assigned to the unbound NHC groups according to the literature since the N 1s core levels of surface-bound NHC are ∼1 eV lower than those of unbound NHC.[38,42] Interestingly, the area of the peak at 401.3 eV in the N 1s region was the largest in the spectra of the **NHC15AZO** monolayer generated from the 1.00 mM solution and gradually decreased when the adsorbate concentrations were reduced. Based on these peak area values, we used the N 1s region of the spectra to determine the degrees of bound/unbound NHC on gold. For the NHC SAMs generated from the high solution concentration (1.00 mM), the areas of peaks at 399.8 and 401.3 eV are close to each other with a ratio of ∼58:42, while the area of peak at 401.3 eV disappeared for the SAMs derived from the low solution concentration (0.01 mM), consistent with a model in which all (or almost all) of the NHC moieties were bound to the gold surface.

Moreover, for quantitative analysis of the NHC bindings on gold substrates, the percentages of bound nitrogen for each **NHC15AZO** SAM were determined by deconvolution of the N 1s region in the XPS spectra (detailed deconvolution graphs and calculations are shown in Figure 2b and Table S1). The percentage of bound N was calculated using the intensities of the peaks at 399.8 and 401.3 eV and compared to percentage of bound N at 0.01 mM (assuming that the NHC groups on the **NHC15AZO** SAM obtained from the 0.01 mM solution are fully bound to the gold). The data show that the percentage of bound nitrogen in the **NHC15AZO** SAMs decreased upon increasing the concentration of the adsorbate solution. Specifically, bound nitrogen constituted 58, 71, and 100% of the nitrogen in the SAMs obtained from 1.00, 0.10, and 0.01 mM solutions, respectively. In particular, the

percentage of bound nitrogen in the monolayer generated from **NHC15AZO** at 1.00 mM was approximately half (~58%) of that at 0.01 mM. This observation is consistent with a model of the **NHC15AZO** SAMs generated from the 1.00 mM solution where only one NHC headgroup in the bidentate adsorbate **NHC15AZO** is bound to gold while the other NHC moiety is exposed to air. This interpretation is consistent with that obtained from the ellipsometric thickness data described in the previous section.

The O 1s XPS spectra of the **NHC15AZO** SAMs generated from adsorbate solutions of varying concentration are provided in Figure 2c. Apparently, the intensity of the peak at 532.6 eV, which corresponds to the oxygen atoms of C=O/S=O and C−O,[62−65] diminished when the concentration of the adsorbate solution was decreased, while the peak intensity at 530.3 eV, which may be assigned to gold oxide layers,[66] was increased. The difference in peak intensities of **NHC15AZO** SAMs generated from different adsorbate concentration solutions can be rationalized because the signal arising from the oxygen atoms in the ester and ether groups of the SAMs can plausibly become attenuated as the concentration of the **NHC15AZO[OMs]** adsorbate decreases due to the differing orientations of the adsorbate molecules on the surface (i.e., linear at high concentration vs hairpin at low concentration).

To quantify the orientations of **NHC15AZO** molecules in each monolayer, the relative atomic concentrations of each film were determined using the oxygen-to-gold ratio (O/Au) derived from the peak areas of O 1s at 532.6 eV and Au 4f (see Table S2 for the detailed calculations). For comparison, the number of atoms in the **NHC15AZO** film generated from the 1.00 mM solution was assumed to be 100%, and the peak areas of monolayers obtained from the 0.10 and 0.01 mM solutions were normalized to that obtained from the 1.00 mM solution. Additionally, the relative atomic concentrations of carbon and nitrogen on each SAM were also calculated using the same method. Figure 2d presents the changes in the percentages of the relative atomic concentrations as functions of the adsorbate concentration in the deposition solutions. Specifically, the relative atomic concentrations of the monolayer decrease as the concentrations are lowered, with the relative atomic concentrations of the SAM formed from the 0.01 mM solution being roughly half that of the SAM generated from the 1.00 mM solution (54% for C, 57% for N, and 39% for O). Notably, due to the presence of oxygen atoms in the mesylate anions atop the monolayer obtained from the 1.00 mM solution (linear orientation), the difference in signal intensity of the O atoms in the SAM generated from the 0.01 mM solution (hairpin orientation) was remarkably greater than the difference in signal intensity of the N atoms in the SAM (linear vs hairpin). This trend is consistent with the data of the thicknesses observed by ellipsometry (e.g., the thickness of films generated from the highly concentrated 1.00 mM solution was 17 Å while that of the SAMs generated from the less concentrated 0.01 mM solution was 9 Å). Thus, thick films were formed in the 1.00 mM solution, while thin films were generated in the 0.01 mM solution.

PM-IRRAS Analysis. Figure 3 shows the PM-IRRAS spectra of the **NHC15AZO** monolayers generated from solutions of varying concentrations of **NHC15AZO[OMs]** (1.00, 0.10, and 0.01 mM). The $\nu_a^{CH_2}$ band positions for all of the **NHC15AZO** films appeared at 2927 cm^{-1}, which is similar to the position of the **NHC15OH** SAMs (see Table 1). This high wavenumber shows that the NHC-based monolayers are less conformation-
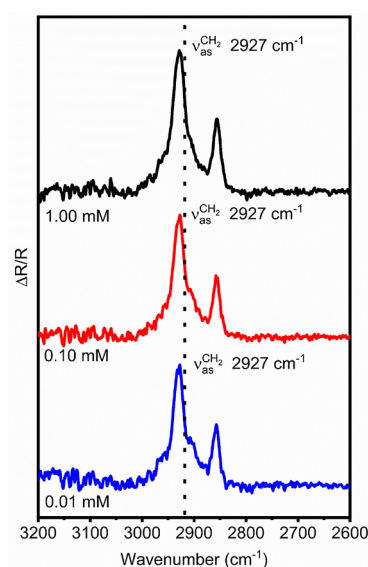

Figure 3. PM-IRRAS spectra for the C−H stretching region obtained from the **NHC15AZO** SAMs generated from the 1.00, 0.10, and 0.01 mM solutions of the **NHC15AZO[OMs]**. The asymmetric methylene stretching vibration values were obtained from three independent sets of experiments, and the reproducibility of the values was within ±1 cm^{-1}. The dotted line marks the 2918 cm^{-1} value corresponding to the well-ordered SAMs with the hydrocarbon chains having a fully trans-extended conformation.

ally ordered than the films derived from normal alkanethiols. Such a difference in the band positions between alkanethiol monolayers and NHC-based SAMs can be attributed to the difference in their surface coverages on gold surfaces due to the steric hindrance of the substituted benzimidazole-based NHC headgroups. In fact, substituted imidazole-based SAMs on gold have lower surface coverages than thiol-based SAMs.[19,20,25] Thus, the steric bulk of the headgroups might be responsible for preventing the kind of dense alkyl packing found in thiol-based SAMs.[55,67]

Interestingly, the band positions for the $\nu_a^{CH_2}$ of all **NHC15AZO** monolayers appeared at 2927 cm^{-1} regardless of the concentration of the adsorbate solutions used in the SAM preparations in this study. Since the packing density of adsorbate molecules on SAMs influences their conformational order on the surfaces,[68−70] these data can be interpreted to indicate that the **NHC15AZO[OMs]** adsorbates generate SAMs on gold in which the alkyl chains lack conformational order and instead form liquid-like (i.e., conformationally floppy) structures on the surface of gold because of the larger on-surface separation enforced by the NHC headgroups. Notably, this model is consistent with the data obtained by ellipsometry and by XPS.

*Analysis of Molecular Orientations of SAMs Generated from Solutions of Varying Concentrations of the **NHC15A-ZO** Absorbate Based on SEM Images.* To provide additional support for the effect of the adsorbate concentration on the molecular orientations of the **NHC15AZO** adsorbate on gold, we exposed the **NHC15AZO** SAMs generated from solutions at three adsorbate concentrations (i.e., 1.00, 0.10, and 0.01 mM) to excess gold nanoparticles (AuNPs). Since NHCs have been shown to bind to AuNPs,[22] we used them as tags to model the free NHC groups on the NHC SAM surfaces.[71] The AuNPs bound on the SAM surfaces were observed as white
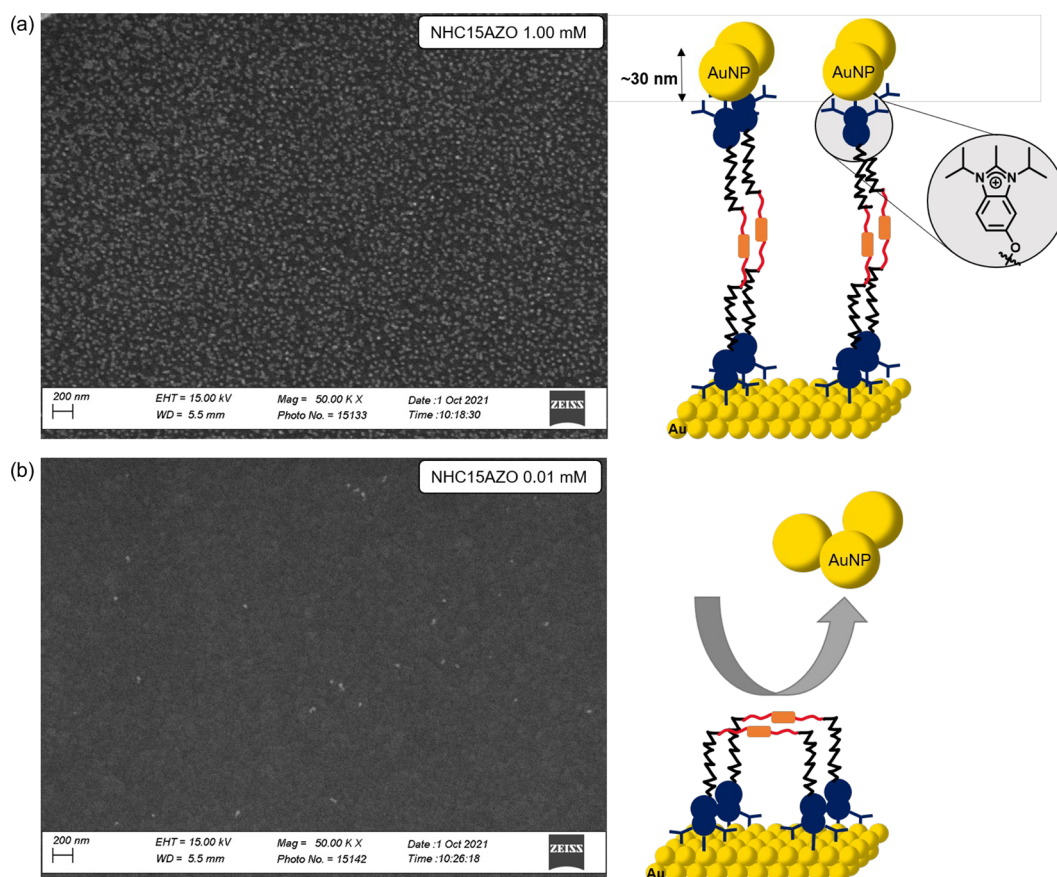
Figure 4. SEM images of gold nanoparticles immobilized on **NHC15AZO** SAMs generated from (a) 1.00 and (b) 0.01 mM adsorbate solutions. Illustrations are the hypothesized orientations of **NHC15AZO** molecules on the SAMs on gold surfaces.
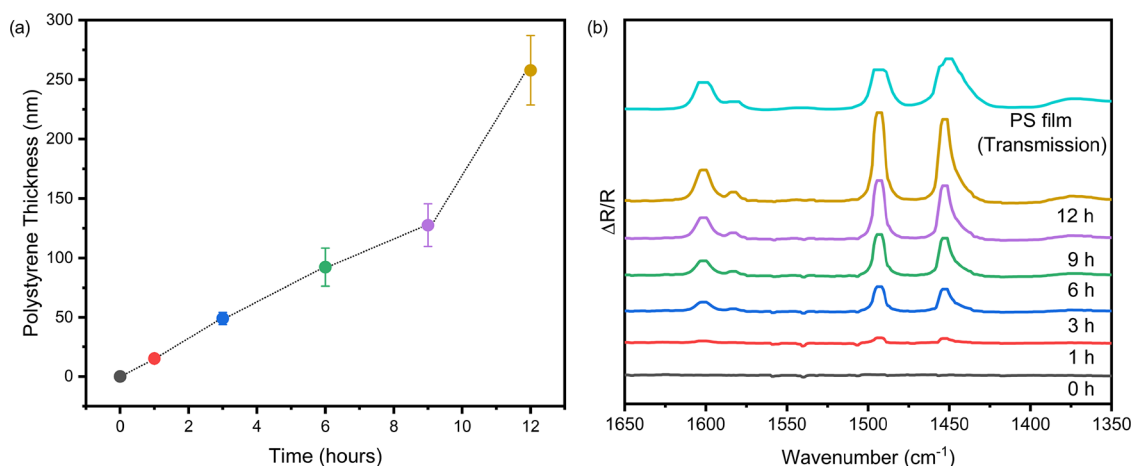

Figure 5. (a) Thicknesses of polystyrene brushes as a function of irradiation time. (b) PM-IRRAS spectra of the C=C bond stretching region of the polystyrene brushes grown from **NHC15AZO** SAMs on gold substrates.

dots from a black background in scanning electron microscopy (SEM) images (see Figure 4 and Figure S8).

We also prepared a reference surface by depositing AuNPs on a preformed 1,6-hexanedithiol SAM and analyzed the surface by SEM (Figure S8a).[11] In these SEM experiments, we observed regularly dispersed AuNPs on the surface of the 1,6-hexanedithiol SAM and the **NHC15AZO** SAM generated from the 1.00 mM solution but almost no AuNPs on the SAM fabricated at the lowest concentration (0.01 mM). Thus, the SEM images in Figure 4 and Figure S8 strongly support the

adsorbate conformations of **NHC15AZO** SAMs: in the linear conformation, one NHC headgroup of the **NHC15AZO** molecules binds to the gold substrate, and the other NHC is exposed to the air where it can bind to AuNPs; on the other hand, AuNPs fail to attach to the hairpin conformation due to the absence of unbound NHC groups on the surfaces of the hairpin SAMs. These results are consistent with the ellipsometry, XPS, and PM-IRRAS data presented in the previous sections.

Growth of Polystyrene Brushes with Well-Controlled Thickness from NHC15AZO SAMs on Gold Surfaces Simply by Varying the Reaction Time. The potential application of the new azo-initiator NHC SAMs as platforms for surface-initiated polymerizations was demonstrated by photoinitiated radical polymerizations of polystyrene. The photoinitiated polymerizations of polystyrene on hairpin **NHC15AZO** monolayers obtained from the 0.01 mM solution were conducted in neat styrene under 365 nm UV light irradiation. The ellipsometric thicknesses of the growing polystyrene films were monitored as a function of irradiation time and are shown in Figure 5a. Notably, the thickness of polystyrene brushes generated from **NHC15AZO** SAMs linearly increased when the irradiation time increased. Moreover, the intensities of the C=C double bond stretching vibration peaks in the PM-IRRAS spectra of the growing polystyrenes as a function of time are shown in Figure 5b. The peaks at 1450, 1500, and 1600 cm^{-1} are attributed to the C=C bond in the aromatic rings of polystyrene films.[72] The increase in intensities of those peaks shows that not only were polystyrene brushes successfully grown from the **NHC15AZO** SAMs on gold but also that the styrene content of the films increased during the radical polymerization. Thus, the newly developed radical initiator **NHC15AZO** SAMs with hairpin conformations on the surface of gold provide convenient platforms for growing surface-initiated polymers in which the film thickness can be tuned simply by adjusting the reaction time. Importantly, the growth of these films can be tuned to give markedly greater polymer thicknesses than those generated using other NHC-based adsorbates (e.g., 250 nm vs 2 nm).[25,26]

We also used atomic force microscopy (AFM) to evaluate the surface morphology of grown polystyrene films from **NHC15AZO** monolayers on gold substrates at different UV irradiation times. The 2D and corresponding 3D AFM images of the original **NHC15AZO** SAM (at 0 h) and polymer films obtained after 6 and 12 h of UV irradiation are shown in Figure 6. The AFM image at 0 h (Figure 6a) shows a uniform
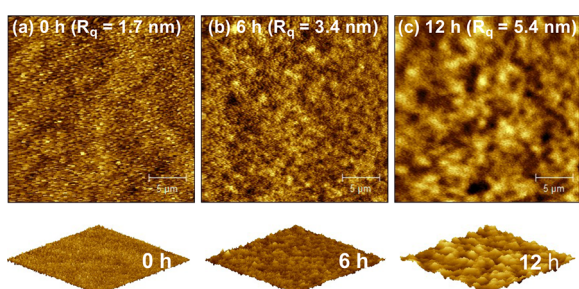

Figure 6. AFM images of the **NHC15AZO** SAM on a gold flat surface: (a) 0 h and grown polystyrene brushes via photoinitiated radical polymerization using 365 nm UV light after (b) 6 and (c) 12 h: 2D (top) and 3D (bottom) views (25 × 25 μm).

flat surface with a root-mean-square surface roughness (R_q) of ~1.7 nm of the **NHC15AZO** SAM on gold generated from the 0.01 mM solution. The polystyrene film grown after 6 h of polymerization was less uniform than the **NHC15AZO** SAM surface, with an R_q value of ~3.4 nm (Figure 6b). After 12 h of polymerization, the surface roughness of the grown polystyrene film increased to ~5.4 nm (Figure 6c). Importantly, the AFM images show that highly dense polymer brush films can be grown from **NHC15AZO** SAMs on gold surfaces.

CONCLUSIONS

This work demonstrates a reliable and convenient method of preparing high-quality NHC SAMs on gold substrates via the direct deposition of bench-stable NHC methanesulfonate salts in methanol solutions at room temperature under an ambient atmosphere. The resulting NHC monolayers were characterized by ellipsometry, XPS, PM-IRRAS, and contact angle measurements, and their quality was identical to that of the SAMs prepared from NHC bicarbonate adsorbates. Due to the simple and mild conditions of SAM formation, the method can potentially allow for the incorporation of a variety of functional groups on NHC SAM-based surfaces. Based on these findings, a new radical initiator α,ω-bidentate azo-terminated NHC adsorbate **NHC15AZO[OMs]** was designed and synthesized and then used to prepare NHC SAMs on gold substrates with both headgroups bound to the surface, allowing unique tethering of all of the azo radical initiator sites on the substrate. Consequently, no surface-unbound free polymer chains were generated during the photoinitiated radical styrene polymer growth processes using 365 nm UV light on the **NHC15AZO** SAM surfaces. Moreover, our new NHC-based initiator can provide strong C–Au bonding through both NHC headgroups of the molecule on the gold surfaces. The molecular orientations of **NHC15AZO** SAMs were studied by ellipsometry, XPS, PM-IRRAS, and SEM based on interactions between the radical initiator monolayers and gold nanoparticles. Notably, polystyrene films with well-controlled thicknesses were generated from our radical initiator **NHC15AZO** monolayers on gold substrates by simply adjusting the reaction time, showing that this newly designed NHC radical initiator adsorbate provides a good approach for surface-initiated polymerizations. Due to the potentially wide applications and high stability of NHC-based monolayers, the newly developed convenient method to prepare NHC-based SAMs using NHC methanesulfonate absorbates and surface-initiated polymerizations on NHC SAM surfaces offers a new pathway to develop the next generation of nanocoating materials.

ASSOCIATED CONTENT

Ⓢ Supporting Information

The Supporting Information is available free of charge at https://pubs.acs.org/doi/10.1021/acsami.2c10985.

Synthesis of **NHC15OH[OMs]** and **NHC5AZO[OMs]** (Scheme S1), thickness distribution of **NHC15** SAMs (Figure S1), ion-exchange of **NHC15AZO[I]** (Scheme S2), comparison of **NHC15OH** SAMs generated from **NHC15OH[OMs]** and **NHC15OH[HCO$_3$]** (Figure S2), XPS survey of **NHC15OH** SAMs generated from **NHC15OH[OMs]** and **NHC15OH[HCO$_3$]** (Figure S3), ^{1}H-NMR spectra of **NHC15OH[OMs]** and **NHC15AZO[OMs]** before and after ion-exchange (Figure S4), ^{1}H-NMR spectra of **NHC15OH[OMs]** and **NHC15AZO[OMs]** (Figure S5), deconvolution of XPS C 1s from **NHC15AZO** SAMs (Figure S6), deconvolution of XPS N 1s from **NHC15AZO** SAMs (Figure S7), percentage of bound and unbound nitrogen of **NHC15AZO** SAMs (Table S1), relative atomic concentrations of **NHC15AZO** SAMs (Table S2), SEM images of gold nanoparticles on 1,6-hexanedithiol and **NHC15AZO** monolayers (Figure S8), ^{1}H NMR spectrum of compound **5** (Figure S9), ^{13}C NMR

spectrum of compound **5** (Figure S10), ^{1}H NMR spectrum of compound **6** (Figure S11), ^{13}C NMR spectrum of compound **6** (Figure S12), ^{1}H NMR spectrum of compound **7** (Figure S13), ^{13}C NMR spectrum of compound **7** (Figure S14), ^{1}H spectrum of **NHC15OH[OMs]** (Figure S15), ^{13}C NMR spectrum of **NHC15OH[OMs]** (Figure S16), ^{1}H NMR spectrum of **NHC15AZO[OMs]** (Figure S17), ^{13}C NMR spectrum of **NHC15AZO[OMs]** (Figure S18), high-resolution mass spectroscopy spectra of **NHC15OH[OMs]** (Figure S19), and high-resolution mass spectroscopy spectra of **NHC15AZO[OMs]** (Figure S20) (PDF)

■ AUTHOR INFORMATION

Corresponding Author

T. Randall Lee − *Department of Chemistry and the Texas Center for Superconductivity, University of Houston, Houston, Texas 77204-5003, United States;* orcid.org/0000-0001-9584-8861; Email: trlee@uh.edu

Authors

Yunsoo Choi − *Department of Chemistry and the Texas Center for Superconductivity, University of Houston, Houston, Texas 77204-5003, United States*

Chul Soon Park − *Department of Chemistry and the Texas Center for Superconductivity, University of Houston, Houston, Texas 77204-5003, United States*

Hung-Vu Tran − *Department of Chemistry and the Texas Center for Superconductivity, University of Houston, Houston, Texas 77204-5003, United States;* orcid.org/0000-0001-8536-2737

Chien-Hung Li − *Department of Medicinal and Applied Chemistry, Kaohsiung Medical University, Kaohsiung 807, Taiwan;* orcid.org/0000-0003-1643-8368

Cathleen M. Crudden − *Department of Chemistry, Queen's University, Kingston, Ontario K7L 3N6, Canada;* orcid.org/0000-0003-2154-8107

Complete contact information is available at:
https://pubs.acs.org/10.1021/acsami.2c10985

Notes

The authors declare no competing financial interest.

■ ACKNOWLEDGMENTS

■ REFERENCES

(1) Navarro, L. A.; Enciso, A. E.; Matyjaszewski, K.; Zauscher, S. Enzymatically Degassed Surface-Initiated Atom Transfer Radical Polymerization with Real-Time Monitoring. *J. Am. Chem. Soc.* **2019**, *141*, 3100−3109.

(2) Valencia, L.; Kumar, S.; Jalvo, B.; Mautner, A.; Salazar-Alvarez, G.; Mathew, A. P. Fully Bio-Based Zwitterionic Membranes with Superior Antifouling and Antibacterial Properties Prepared via Surface-Initiated Free-Radical Polymerization of Poly(Cysteine Methacrylate). *J. Mater. Chem. A* **2018**, *6*, 16361−16370.

(3) Jesmer, A. H.; Huynh, V.; Marple, A. S. T.; Ding, X.; Moran-Mirabal, J. M.; Wylie, R. G. Graft-Then-Shrink: Simultaneous Generation of Antifouling Polymeric Interfaces and Localized Surface Plasmon Resonance Biosensors. *ACS Appl. Mater. Interfaces* **2021**, *13*, 52362−52373.

(4) Madsen, J.; Ducker, R. E.; Al Jaf, O.; Cartron, M. L.; Alswieleh, A. M.; Smith, C. H.; Hunter, C. N.; Armes, S. P.; Leggett, G. J. Fabrication of Microstructured Binary Polymer Brush "Corrals" with Integral pH Sensing for Studies of Proton Transport in Model Membrane Systems. *Chem. Sci.* **2018**, *9*, 2238−2251.

(5) Kim, S.; Kwak, D. H.; Choi, I.; Hwang, J.; Kwon, B.; Lee, E.; Ye, J.; Lim, H.; Cho, K.; Chung, H. J.; Lee, W. H. Enhanced Gas Sensing Properties of Graphene Transistor by Reduced Doping with Hydrophobic Polymer Brush as a Surface Modification Layer. *ACS Appl. Mater. Interfaces* **2020**, *12*, 55493−55500.

(6) Zhou, M.; Liu, R.; Jia, D.; Cui, Y.; Liu, Q.; Liu, S.; Wu, D. Ultrathin Yet Robust Single Lithium-Ion Conducting Quasi-Solid-State Polymer-Brush Electrolytes Enable Ultralong-Life and Dendrite-Free Lithium-Metal Batteries. *Adv. Mater.* **2021**, *33*, 2100943.

(7) Weltz, J. S.; Kienle, D. F.; Schwartz, D. K.; Kaar, J. L. Dramatic Increase in Catalytic Performance of Immobilized Lipases by Their Stabilization on Polymer Brush Supports. *ACS Catal.* **2019**, *9*, 4992−5001.

(8) Wu, Y.; Yang, G.; Lin, M.; Kong, X.; Mi, L.; Liu, S.; Chen, G.; Tian, Y.; Jiang, L. Continuously Tunable Ion Rectification and Conductance in Submicrochannels Stemming from Thermoresponsive Polymer Self-Assembly. *Angew. Chem., Int. Ed.* **2019**, *58*, 12481−12485.

(9) Reese, C. J.; Boyes, S. G. New Methods in Polymer Brush Synthesis: Non-Vinyl-Based Semiflexible and Rigid-Rod Polymer Brushes. *Prog. Polym. Sci.* **2021**, *114*, No. 101361.

(10) Zoppe, J. O.; Ataman, N. C.; Mocny, P.; Wang, J.; Moraes, J.; Klok, H. A. Surface-Initiated Controlled Radical Polymerization: State-of-the-Art, Opportunities, and Challenges in Surface and Interface Engineering with Polymer Brushes. *Chem. Rev.* **2017**, *117*, 1105−1318.

(11) Lee, H. J.; Jamison, A. C.; Lee, T. R. Entropy-Driven Conformational Control of α,ω-Difunctional Bidentate-Dithiol Azo-Based Adsorbates Enables the Fabrication of Thermally Stable Surface-Grafted Polymer Films. *ACS Appl. Mater. Interfaces* **2016**, *8*, 15691−15699.

(12) Kuzmyn, A. R.; Teunissen, L. W.; Fritz, P.; van Lagen, B.; Smulders, M. M. J.; Zuilhof, H. Diblock and Random Antifouling Bioactive Polymer Brushes on Gold Surfaces by Visible-Light-Induced Polymerization (SI-PET-RAFT) in Water. *Adv. Mater. Interfaces* **2022**, *9*, 2101784.

(13) Carbonell, C.; Valles, D.; Wong, A. M.; Carlini, A. S.; Touve, M. A.; Korpanty, J.; Gianneschi, N. C.; Braunschweig, A. B. Polymer Brush Hypersurface Photolithography. *Nat. Commun.* **2020**, *11*, 1244.

(14) Love, J. C.; Estroff, L. A.; Kriebel, J. K.; Nuzzo, R. G.; Whitesides, G. M. Self-Assembled Monolayers of Thiolates on Metals as a Form of Nanotechnology. *Chem. Rev.* **2005**, *105*, 1103−1170.

(15) Marquez, M. D.; Zenasni, O.; Rodriguez, D.; Yu, T.; Sakunkaewkasem, S.; Toro Figueira, F.; Czader, A.; Baldelli, S.; Lee, T. R. Burying the Inverted Surface Dipole: Self-Assembled Monolayers Derived from Alkyl-Terminated Partially Fluorinated Alkanethiols. *Chem. Mater.* **2020**, *32*, 953−968.

(16) St. Hill, L. R.; Tran, H.-V.; Chinwangso, P.; Lee, H. J.; Marquez, M. D.; Craft, J. W.; Lee, T. R. Antifouling Studies of Unsymmetrical Oligo(ethylene glycol) Spiroalkanedithiol Self-Assembled Monolayers. *Micro* **2021**, *1*, 151−163.

(17) St. Hill, L. R.; Craft, J. W.; Chinwangso, P.; Tran, H.-V.; Marquez, M. D.; Lee, T. R. Antifouling Coatings Generated from Unsymmetrical Partially Fluorinated Spiroalkanedithiols. *ACS Appl. Bio Mater.* **2021**, *4*, 1563−1572.

(18) Jiang, C.; Wang, G.; Hein, R.; Liu, N.; Luo, X.; Davis, J. J. Antifouling Strategies for Selective in Vitro and in Vivo Sensing. *Chem. Rev.* **2020**, *120*, 3852−3889.

(19) Crudden, C. M.; Horton, J. H.; Ebralidze, I. I.; Zenkina, O. V.; McLean, A. B.; Drevniok, B.; She, Z.; Kraatz, H. B.; Mosey, N. J.; Seki, T.; Keske, E. C.; Leake, J. D.; Rousina-Webb, A.; Wu, G. Ultra Stable

Self-Assembled Monolayers of *N*-Heterocyclic Carbenes on Gold. *Nat. Chem.* **2014**, *6*, 409−414.

(20) Crudden, C. M.; Horton, J. H.; Narouz, M. R.; Li, Z.; Smith, C. A.; Munro, K.; Baddeley, C. J.; Larrea, C. R.; Drevniok, B.; Thanabalasingam, B.; McLean, A. B.; Zenkina, O. V.; Ebralidze, I. I.; She, Z.; Kraatz, H. B.; Mosey, N. J.; Saunders, L. N.; Yagi, A. Simple Direct Formation of Self-Assembled *N*-Heterocyclic Carbene Monolayers on Gold and Their Application in Biosensing. *Nat. Commun.* **2016**, *7*, 12654.

(21) Cristina, L. J.; Ruano, G.; Salvarezza, R.; Ferrón, J. Thermal Stability of Self-Assembled Monolayers of n-Hexanethiol on Au(111)-(1 × 1) and Au(001)-(1 × 1). *J. Phys. Chem. C* **2017**, *121*, 27894−27904.

(22) Smith, C. A.; Narouz, M. R.; Lummis, P. A.; Singh, I.; Nazemi, A.; Li, C. H.; Crudden, C. M. *N*-Heterocyclic Carbenes in Materials Chemistry. *Chem. Rev.* **2019**, *119*, 4986−5056.

(23) Koy, M.; Bellotti, P.; Das, M.; Glorius, F. *N*-Heterocyclic Carbenes as Tunable Ligands for Catalytic Metal Surface. *Nat. Catal.* **2021**, *4*, 352−363.

(24) Bellotti, P.; Koy, M.; Hopkinson, M. N.; Glorius, F. Recent Advances in the Chemistry and Applications of *N*-Heterocyclic Carbenes. *Nat. Rev. Chem.* **2021**, *5*, 711−725.

(25) Zhukhovitskiy, A. V.; Mavros, M. G.; Van Voorhis, T.; Johnson, J. A. Addressable Carbene Anchors for Gold Surfaces. *J. Am. Chem. Soc.* **2013**, *135*, 7418−7421.

(26) Berg, I.; Einav, A.; Hale, L.; Toste, F. D.; Gross, E. *N*-Heterocyclic Carbene Based Nanolayer for Copper Film Oxidation Mitigation. *Angew. Chem., Int. Ed.* **2022**, *61*, No. e202201093. and references therein

(27) Fèvre, M.; Pinaud, J.; Leteneur, A.; Gnanou, Y.; Vignolle, J.; Taton, D.; Miqueu, K.; Sotiropoulos, J. M. Imidazol(in)Ium Hydrogen Carbonates as a Genuine Source of *N*-Heterocyclic Carbenes (NHCs): Applications to the Facile Preparation of NHC Metal Complexes and to NHC-Organocatalyzed Molecular and Macromolecular Syntheses. *J. Am. Chem. Soc.* **2012**, *134*, 6776−6784.

(28) She, Z.; Narouz, M. R.; Smith, C. A.; Maclean, A.; Loock, H. P.; Kraatz, H. B.; Crudden, C. M. *N*-Heterocyclic Carbene and Thiol Micropatterns Enable the Selective Deposition and Transfer of Copper Films. *Chem. Commun.* **2020**, *56*, 1275−1278.

(29) Li, Z.; Munro, K.; Narouz, M. R.; Lau, A.; Hao, H.; Crudden, C. M.; Horton, J. H. Self-Assembled *N*-Heterocyclic Carbene-Based Carboxymethylated Dextran Monolayers on Gold as a Tunable Platform for Designing Affinity-Capture Biosensor Surfaces. *ACS Appl. Mater. Interfaces* **2018**, *10*, 17560−17570.

(30) Wang, G.; Rühling, A.; Amirjalayer, S.; Knor, M.; Ernst, J. B.; Richter, C.; Gao, H. J.; Timmer, A.; Gao, H. Y.; Doltsinis, N. L.; Glorius, F.; Fuchs, H. Ballbot-Type Motion of *N*-Heterocyclic Carbenes on Gold Surfaces. *Nat. Chem.* **2017**, *9*, 152−156.

(31) Bakker, A.; Timmer, A.; Kolodzeiski, E.; Freitag, M.; Gao, H. Y.; Mönig, H.; Amirjalayer, S.; Glorius, F.; Fuchs, H. Elucidating the Binding Modes of *N*-Heterocyclic Carbenes on a Gold Surface. *J. Am. Chem. Soc.* **2018**, *140*, 11889−11892.

(32) Qi, S.; Ma, Q.; He, X.; Tang, Y. Self-Assembled Monolayers of *N*-Heterocyclic Carbene on Gold: Stability under Ultrasonic Circumstance and Computational Study. *Colloids Surf., A* **2018**, *538*, 488−493.

(33) Larrea, C. R.; Baddeley, C. J.; Narouz, M. R.; Mosey, N. J.; Horton, J. H.; Crudden, C. M. *N*-Heterocyclic Carbene Self-Assembled Monolayers on Copper and Gold: Dramatic Effect of Wingtip Groups on Binding, Orientation and Assembly. *ChemPhysChem* **2017**, *18*, 3536−3539.

(34) Dery, S.; Kim, S.; Tomaschun, G.; Haddad, D.; Cossaro, A.; Verdini, A.; Floreano, L.; Klüner, T.; Toste, F. D.; Gross, E. Flexible NO₂-Functionalized *N*-Heterocyclic Carbene Monolayers on Au(111) Surface. *Chem. - A Eur. J.* **2019**, *2*, 15067−15072.

(35) Lovat, G.; Doud, E. A.; Lu, D.; Kladnik, G.; Inkpen, M. S.; Steigerwald, M. L.; Cvetko, D.; Hybertsen, M. S.; Morgante, A.; Roy, X.; Venkataraman, L. Determination of the Structure and Geometry

of *N*-Heterocyclic Carbenes on Au(111) Using High-Resolution Spectroscopy. *Chem. Sci.* **2019**, *10*, 930−935.

(36) Li, Z.; Narouz, M. R.; Munro, K.; Hao, B.; Crudden, C. M.; Horton, J. H.; Hao, H. Carboxymethylated Dextran-Modified *N*-Heterocyclic Carbene Self-Assembled Monolayers on Gold for Use in Surface Plasmon Resonance Biosensing. *ACS Appl. Mater. Interfaces* **2017**, *9*, 39223−39234.

(37) Li, Z.; Munro, K.; Ebralize, I. I.; Narouz, M. R.; Padmos, J. D.; Hao, H.; Crudden, C. M.; Horton, J. H. *N*-Heterocyclic Carbene Self-Assembled Monolayers on Gold as Surface Plasmon Resonance Biosensors. *Langmuir* **2017**, *33*, 13936−13944.

(38) Nguyen, D. T.; Freitag, M.; Körsgen, M.; Lamping, S.; Rühling, A.; Schäfer, A. H.; Siekman, M. H.; Arlinghaus, H. F.; van der Wiel, W. G.; Glorius, F.; Ravoo, B. J. Versatile Micropatterns of *N*-Heterocyclic Carbenes on Gold Surfaces: Increased Thermal and Pattern Stability with Enhanced Conductivity. *Angew. Chem., Int. Ed.* **2018**, *57*, 11465−11469.

(39) Kang, S.; Park, S.; Kang, H.; Cho, S. J.; Song, H.; Yoon, H. J. Tunneling and Thermoelectric Characteristics of *N*-Heterocyclic Carbene-Based Large-Area Molecular Junctions. *Chem. Commun.* **2019**, *55*, 8780−8783.

(40) Kim, H. K.; Hyla, A. S.; Winget, P.; Li, H.; Wyss, C. M.; Jordan, A. J.; Larrain, F. A.; Sadighi, J. P.; Fuentes-Hernandez, C.; Kippelen, B.; Brédas, J. L.; Barlow, S.; Marder, S. R. Reduction of the Work Function of Gold by *N*-Heterocyclic Carbenes. *Chem. Mater.* **2017**, *29*, 3403−3411.

(41) Lv, A.; Freitag, M.; Chepiga, K. M.; Schäfer, A. H.; Glorius, F.; Chi, L. *N*-Heterocyclic-Carbene-Treated Gold Surfaces in Pentacene Organic Field-Effect Transistors: Improved Stability and Contact at the Interface. *Angew. Chem., Int. Ed.* **2018**, *57*, 4792−4796.

(42) Nguyen, D. T.; Freitag, M.; Gutheil, C.; Sotthewes, K.; Tyler, B. J.; Böckmann, M.; Das, M.; Schlüter, F.; Doltsinis, N. L.; Arlinghaus, H. F.; Ravoo, B. J.; Glorius, F. An Arylazopyrazole-Based *N*-Heterocyclic Carbene as a Photoswitch on Gold Surfaces: Light-Switchable Wettability, Work Function, and Conductance. *Angew. Chem., Int. Ed.* **2020**, *59*, 13651−13656.

(43) Weidner, T.; Baio, J. E.; Mundstock, A.; Grosse, C.; Karthaeuser, S.; Bruhn, C.; Siemeling, U. NHC-Based Self-Assembled Monolayers on Solid Gold Substrates. *Aust. J. Chem.* **2011**, *64*, 1177−1179.

(44) Amit, E.; Dery, L.; Dery, S.; Kim, S.; Roy, A.; Hu, Q.; Gutkin, V.; Eisenberg, H.; Stein, T.; Mandler, D.; Dean Toste, F.; Gross, E. Electrochemical Deposition of *N*-Heterocyclic Carbene Monolayers on Metal Surfaces. *Nat. Commun.* **2020**, *11*, 5714.

(45) Otera, J. Transesterification. *Chem. Rev.* **1993**, *93*, 1449−1470.

(46) Dejesus, J. F.; Trujillo, M. J.; Camden, J. P.; Jenkins, D. M. *N*-Heterocyclic Carbenes as a Robust Platform for Surface-Enhanced Raman Spectroscopy. *J. Am. Chem. Soc.* **2018**, *140*, 1247−1250.

(47) Fèvre, M.; Coupillaud, P.; Miqueu, K.; Sotiropoulos, J. M.; Vignolle, J.; Taton, D. Imidazolium Hydrogen Carbonates versus Imidazolium Carboxylates as Organic Precatalysts for *N*-Heterocyclic Carbene Catalyzed Reactions. *J. Org. Chem.* **2012**, *77*, 10135−10144.

(48) Zhou, Y.; Zhang, Z.; Postma, A.; Moad, G. Kinetics and Mechanism for Thermal and Photochemical Decomposition of 4,4′-Azobis(4-Cyanopentanoic Acid) in Aqueous Media. *Polym. Chem.* **2019**, *10*, 3284−3287.

(49) Sakunkaewkasem, S.; Marquez, M. D.; Lee, H. J.; Lee, T. R. Mixed Phase-Incompatible Monolayers: Toward Nanoscale Anti-Adhesive Coatings. *ACS Appl. Nano Mater.* **2020**, *3*, 4091−4101.

(50) Chinwangso, P.; Lee, H. J.; Lee, T. R. Self-Assembled Monolayers Generated from Unsymmetrical Partially Fluorinated Spiroalkanedithiols. *Langmuir* **2015**, *31*, 13341−13349.

(51) Smith, D. K.; Miller, N. R.; Korgel, B. A. Iodide in CTAB Prevents Gold Nanorod Formation. *Langmuir* **2009**, *25*, 9518−9524.

(52) Lee, C.; Josephs, E. A.; Shao, J.; Ye, T. Nanoscale Chemical Patterns on Gold Microplates. *J. Phys. Chem. C* **2012**, *116*, 17625−17632.

(53) Sakunkaewkasem, S.; Gonzalez, M. A.; Marquez, M. D.; Lee, T. R. Olefin-Bridged Bidentate Adsorbates for Generating Self-Assembled Monolayers on Gold. *Langmuir* **2020**, *36*, 10699−10707.

(54) Yu, T.; Marquez, M. D.; Zenasni, O.; Lee, T. R. Mimicking Polymer Surfaces Using Cyclohexyl- and Perfluorocyclohexyl-Terminated Self-Assembled Monolayers. *ACS Appl. Nano Mater.* **2019**, *2*, 5809−5816.

(55) Porter, M. D.; Bright, T. B.; Allara, D. L.; Chidsey, C. E. Spontaneously Organized Molecular Assemblies. 4. Structural Characterization of *n*-Alkyl Thiol Monolayers on Gold by Optical Ellipsometry, Infrared Spectroscopy, and Electrochemistry. *J. Am. Chem. Soc.* **1987**, *109*, 3559−3568.

(56) MacPhail, R. A.; Strauss, H. L.; Snyder, R. G.; Eiliger, C. A. C-H Stretching Modes and the Structure of *n*-Alkyl Chains. 2. Long, All-Trans Chains. *J. Phys. Chem.* **1984**, *88*, 334−341.

(57) Snyder, R. G.; Strauss, H. L.; Elliger, C. A. C-H Stretching Modes and the Structure of *n*-Alkyl Chains. 1. Long, Disordered Chains. *J. Phys. Chem.* **1982**, *86*, 5145−5150.

(58) Kaestle, K. L.; Anwer, M. K.; Audhya, T. K.; Goldstein, G. Cleavage of Esters Using Carbonates and Bicarbonates of Alkali Metals: Synthesis of Thymopentin. *Tetrahedron Lett.* **1991**, *32*, 327−330.

(59) Zhai, G.; Yu, W. H.; Kang, E. T.; Neoh, K. G.; Huang, C. C.; Liaw, D. J. Functionalization of Hydrogen-Terminated Silicon with Polybetaine Brushes via Surface-Initiated Reversible Addition-Fragmentation Chain-Transfer (RAFT) Polymerization. *Ind. Eng. Chem. Res.* **2004**, *43*, 1673−1680.

(60) Park, C. S.; Lee, H. J.; Jamison, A. C.; Lee, T. R. Robust Thick Polymer Brushes Grafted from Gold Surfaces Using Bidentate Thiol-Based Atom-Transfer Radical Polymerization Initiators. *ACS Appl. Mater. Interfaces* **2016**, *8*, 5586−5594.

(61) Yu, W. H.; Kang, E. T.; Neoh, K. G. Functionalization of Hydrogen-Terminated Si(100) Substrate by Surface-Initiated RAFT Polymerization of 4-Vinylbenzyl Chloride and Subsequent Derivatization for Photoinduced Metallization. *Ind. Eng. Chem. Res.* **2004**, *43*, 5194−5202.

(62) Zengin, A.; Caykara, T. RAFT-Mediated Synthesis of Poly[(oligoethylene glycol) methyl ether acrylate] Brushes for Biological Functions. *J. Polym. Sci., Part A: Polym. Chem.* **2012**, *50*, 4443−4450.

(63) Barbey, R.; Laporte, V.; Alnabulsi, S.; Klok, H. A. Postpolymerization Modification of Poly(glycidyl methacrylate) Brushes: An XPS Depth-Profiling Study. *Macromolecules* **2013**, *46*, 6151−6158.

(64) Dong, H. B.; Xu, Y. Y.; Yi, Z. Synthesis of an Amphiphilic PPESK-g-P(PEGMA) Graft Copolymer via ATPR and Its Use in Blend Modification of PPESK Membranes. *Chin. J. Polym. Sci.* **2009**, *27*, 813−820.

(65) Wavhal, D. S.; Fisher, E. R. Hydrophilic Modification of Polyethersulfone Membranes by Low Temperature Plasma-Induced Graft Polymerization. *J. Memb. Sci.* **2002**, *209*, 255−269.

(66) Juodkazis, K.; Juodkazyte, J.; Jasulaitiene, V.; Lukinskas, A.; Šebeka, B. XPS Studies on the Gold Oxide Surface Layer Formation. *Electrochem. Commun.* **2000**, *2*, 503−507.

(67) Lee, H. J.; Jamison, A. C.; Yuan, Y.; Li, C. H.; Rittikulsittichai, S.; Rusakova, I.; Lee, T. R. Robust Carboxylic Acid-Terminated Organic Thin Films and Nanoparticle Protectants Generated from Bidentate Alkanethiols. *Langmuir* **2013**, *29*, 10432−10439.

(68) Schreiber, F. Thiol-Based Self-Assembled Monolayers: Structure Of. *Encycl. Mater. Sci. Technol.* **2001**, 9323−9331.

(69) Park, J. S.; Vo, A. N.; Barriet, D.; Shon, Y. S.; Lee, T. R. Systematic Control of the Packing Density of Self-Assembled Monolayers Using Bidentate and Tridentate Chelating Alkanethiols. *Langmuir* **2005**, *21*, 2902−2911.

(70) Garg, N.; Friedman, J. M.; Lee, T. R. Adsorption Profiles of Chelating Aromatic Dithiols and Disulfides: Comparison to Those of Normal Alkanethiols and Disulfides. *Langmuir* **2000**, *16*, 4266−4271.

(71) Kim, Y. H.; Gorman, C. B. Standing up versus Looping over: Controlling the Geometry of Self-Assembled Monolayers of α,ω-Diynes on Gold. *Langmuir* **2011**, *27*, 6069−6075.

(72) Erukhimovich, I.; de la Cruz, M. O. Structural Anisotropy in Friction-Deposited Layers of Polystyrene. *J. Polym. Sci., Part B: Polym. Phys.* **2006**, *44*, 3272−3281.